# Characterization of Novel α-Mangostin and Paeonol Derivatives With Cancer-Selective Cytotoxicity

Suneetha Nunna[1], Ying-Pei Huang[1,2], Mahdi Rasa[1], Anna Krepelova[1], Francesco Annunziata[1], Lisa Adam[1], Sandra Käppel[1], Ming-Hua Hsu[3,4], and Francesco Neri[1]

## ABSTRACT

α-Mangostin (aMan) and Paeonol (Pae) have shown anticancer and anti-inflammatory properties. However, these two natural compounds have no clinical value because of their low solubility and low membrane permeability. In this study, we screened chemically synthesized derivatives from these two natural compounds as potential novel chemicals that increase cancer cell cytotoxicity over nontransformed human cells. We found that two derivative compounds, named α-Mangostin-1 (aMan1) and Paeonol-1 (Pae1) more efficiently and more specifically induced cytotoxicity in HCT116, HT29, and SW48 colorectal cancer cell lines than the parental compounds. Both aMan1 and Pae1 arrested HCT116 cells in the $G_1$ phase and HT29 and SW48 cells in the $G_2$–M phase of the cell cycle. Both aMan1 and Pae1 induced apoptosis in human colorectal cancer cells, through a caspase-dependent mechanism. aMan1 and Pae1 induced selective transcriptional responses in colorectal cancer cells involving genes related to metabolic stress and DNA damage response signaling pathways. Finally, experiments on primary colon organoids showed that both derivatives were able to kill cancer-derived organoids without affecting the viability of organoids derived from healthy tissue, where the parental compounds and the currently used chemotherapeutic drug irinotecan failed. In conclusion, our findings expand the knowledge of natural compound derivatives as anticancer agents and open new avenues of research in the derivation of lead compounds aimed at developing novel chemotherapeutic drugs for colorectal cancer treatment that selectively target cancer, but not healthy cells.

## Introduction

Colorectal cancer is the third most prevalent cancer in the world, a malignancy that is frequently caused by lifestyle, diet, and genetics (1, 2). Colorectal cancer is also an age-related disease with increasing incidence rate with aging, especially after the age of 50. Currently, colorectal cancer has a very differential prognosis. When diagnosed at an early stage, the 5-year survival rate of the patient is 90%; but, it drops to 10% if diagnosed when it has metastasized (3). The current medical colorectal cancer treatments usually include a combination of multiple chemotherapeutic, targeted and/or immunotherapeutic drugs (4, 5). However, such therapies are often inefficient to completely cure colorectal cancer and have numerous and severe side effects on the patients' health. The side effects of drug-mediated therapies depend on the type, dose and duration of the treatment and are usually caused by the lack of a drug's cancer specificity. Because of the severe side effects, chemotherapy is often designed taking into consideration the health status of the patients and their medical history. In recent years, a large effort has been devoted to provide psychologic and medical support to patients dealing with severe side effects (6–8). The high morbidity and mortality associated with colorectal cancer and the inefficacy of the current available drugs to selectively target cancer cells increases the demand to find novel cost-effective anticancer agents.

Natural compounds have emerged as economic, practicable, and effective therapeutic approaches for treatment of cancer. Natural compounds (phytochemicals) are substances with potentially bioactive properties produced by microbes or plants. Phytochemicals have been largely shown to suppress carcinogenesis in studies conducted *in vitro* and in preclinical models. Almost half of the approved chemotherapeutic drugs are derived from natural compounds or their derivatives (9–11). One class of chemical natural phenolic compounds, the xanthonoids, have shown potential anticancer, anti-inflammatory, and antioxidative properties (12,13). Among xanthonoids, the compound α-Mangostin (aMan) derived from *Garcinia mangostana* has been shown to have a broad functional activity. For example, aMan possesses a variety of pharmacologic functions: antioxidant, anticarcinogenic, and antidiabetic—among which, the anticancer activity is the most promising (14). aMan affects tumor cell growth *in vitro* and *in vivo*, including high-grade malignancies. aMan inhibits the migration and invasion and reduces the actin cytoskeleton of human lung cancer cells, thereby exhibiting antimetastatic activity (15). aMan inhibits the activation of TAK1–NF-κB pathway, thus acting as an anti-inflammatory compound (16). It also induces mitochondrial dysfunction (17). Furthermore, it induces apoptosis and cell-cycle arrest in human colon cancer cell lines DLD-1, HCT116, and HT29 (18) and blocks tumor growth in mouse xenograft models (19). Another natural phenolic compound Paeonol (Pae; 2-hydroxy-4-methoxyacetophenone) is a bioactive component isolated from the root bark of *Paeonia suffruticosa Andr* (20–22). Pae has been widely used as an anti-inflammatory drug for repairing oxidative damage and enhancing immunity function. It also reduces the severity of liver fibrosis and prevents ox-LDL–induced endothelial cell apoptosis (23). Pae inhibits the growth of colorectal cancer cell lines HCT116, SW620 and downregulates the expression of COX-2 and PGE2 synthesis in colorectal

[1]Leibniz-Institute on Ageing - Fritz-Lipmann-Institute (FLI), Jena, Germany. [2]Nuclear Science & Technology Development Center, National Tsing Hua University, Hsinchu, Taiwan. [3]Department of Chemistry, National Changhua University of Education, Changhua, Taiwan, ROC. [4]Department of Medical and Applied Sciences, Kaohsiung Medical University, Kaohsiung, Taiwan, ROC.

**Note:** Supplementary data for this article are available at Molecular Cancer Therapeutics Online (http://mct.aacrjournals.org/).

**Corresponding Author:** Francesco Neri, Epigenetics group, Leibniz Institute on Aging - Fritz Lipmann Institute (FLI), Jena, 07745, Germany. E-mail: francesco.neri@unito.it

Mol Cancer Ther 2022;21:257–70

**doi:** 10.1158/1535-7163.MCT-20-0787

cancer LoVo cells (24). Pae significantly lowers tumor growth and causes tumor regression in a gastric cancer cell line of mouse forestomach carcinoma tumor-bearing mice (21). Despite the broad functional activity of aMan and Pae, both of these compounds have an intrinsically low solubility and low membrane permeability that have hindered their clinical use. To improve these properties, novel derivatives of the two compounds could be prepared by adding new functional groups. We speculate that an enhanced solubility and/or improved cell membrane penetration may potentiate their anticancer activity and selectivity as well as increase their therapeutic potential.

This study aimed to improve the cancer cytotoxicity and selectivity of aMan and Pae by the addition of new functional groups. As the cytotoxicity of parental compounds have been tested on colon cancer cell lines and current colon cancer treatments have severe side effects, we investigated the effect of two very promising aMan and Pae derivatives on human colon cancer cell lines and human primary colon organoids. However, other novel compounds may be also of potential interest for the treatment of different types of human cancers. Our findings increase the knowledge regarding natural compound derivatives as anticancer agents and open new research options for the development of lead compounds, such as novel colorectal cancer chemotherapeutic drugs that selectively target cancer, avoiding healthy cells.

## Materials and Methods

### Cell lines and cell viability/cytotoxicity assay

Mycoplasma-free human colon cancer cell lines HCT116 (ATCC, CCL-247), HT29 (ATCC, HTB-38), or SW48 (ATCC, CCL-231) were purchased from ATCC. BjhTERT cells were obtained from collaborators. All the cell lines were cultured in RPMI (GIBCO) supplemented with 10% FCS, 1 mmol/L sodium pyruvate, and 1x Glutamax up to a maximum of 20 passages.

To determine the effect of natural compounds on cell viability, the above-mentioned cell lines (5,000 cells/well) were seeded in a 96-well plate. On the following day, the cells were treated with different concentrations of either aMan (5, 10, 25, and 40 μmol/L) or aMan1 (5, 10, 25, and 40 μmol/L), Pae (100, 200, 300, and 400 μmol/L), or Pae1 (3, 10, 25, and 40 μmol/L) derivatives. The derivative compounds were dissolved in DMSO, and the final concentration of DMSO in the experimental medium was 0.03%. After 72 hours of incubation, the cell supernatant was removed, and the adherent cells were fixed with paraformaldehyde (4%) for 15 minutes and stained with 50 μL of crystal violet blue (0.1%) for 30 minutes at room temperature on an orbital shaker. Then, the cells were washed twice with 200 μL of autoclaved distilled water, and the dye was dissolved in 100 μL of acetic acid (10%). The dissolved dye was transferred to flat-bottom 96-well plates, and the absorbance was measured at 570 nm. The $IC_{50}$ values were calculated using the AAT Bioquest $IC_{50}$ calculator (v.1; ref. 26). For cytotoxicity analysis, MTT assays were performed by following the manufacturing's protocol (MTT Assay Protocol for Cell Viability and Proliferation, Merck, Catalog No. 11465007001). DAPT (Sigma, Catalog No. S2215) was used at the concentration of 30 μmol/L in DMSO.

### Compound synthesis

2-(3,6,8-trihydroxy-2-methoxy-7-(3-methylbut-2-en-1-yl)-9-oxo-9H-xanthen-1-yl) acetaldehyde that we named α-Mangostin-1 (aMan1): a solution of aMan (1 mmol) in methanol (10 mL) and dichloromethane (40 mL) was cooled to −78°C using a dry ice/acetone bath. A stream of ozone was bubbled through the reaction via a gas dispersion tube until the reaction became blue in color (15 minutes). The ozone line was replaced with a stream of nitrogen and bubbling continued for another 15 minutes, by which time the blue color had disappeared. To this solution, dimethyl sulfide (5 mmol) was added in one portion at −78°C, and the cooling bath was removed. The reaction was allowed to warm to room temperature and stirred overnight. The solvent was removed under vacuum, and the residue was purified to by silica gel chromatography (ethyl acetate: hexane = 4: 6) to produce the desired product.

(E)-(4-(3-(2-hydroxy-4-methoxyphenyl)-3-oxoprop-1-en-1-yl) phenyl) boronic acid that we named Paeonol-1 (Pae1): a solution mixture of 2'-hydroxy-4'-methoxyacetophenone (1 mmol) and 4-formylphenylboronic acid (1 mmol) in ethanol (10 mL) was stirred at room temperature for 30 minutes. Then, a solution of 20% (w/w) aqueous KOH (10 mL) was added. The reaction mixture was stirred at room temperature for 12 hours and was monitored by TLC. Afterward, the mixture was poured into ice water acidified with 3N HCl. The solid obtained was filtered and air-dried. Recrystallization from ethanol produced the desired product.

### Apoptosis and cell death analysis by flow cytometry

The BjhTERT, HCT116, HCT116 TP53_KO, HT29, or SW48 cells ($1 \times 10^5$ cells/well) were seeded in a six-well plate. The cells were incubated either with aMan (25 μmol/L), aMan1(25 μmol/L), Pae (300 μmol/L), or Pae1 (10 μmol/L) for 48 hours. For pan-caspase inhibition, the cells were preincubated with pan-caspase inhibitor (20 μmol/L) Z-VAD-FMK (zVAD; Enzo Life Science) for 2 hours, and then the cells were treated with either aMan1 and Pae1 for 48 hours. After incubation, the adherent cells were trypsinized and harvested along with the suspended cells. The cells were washed once with PBS and incubated in 100 μL of 1x Annexin V binding buffer for 20 minutes at room temperature. After washing, the cells were resuspended in PBS supplemented with 0.1% FBS containing DAPI and analyzed by flow cytometry with FACScanto.

### DNA fragmentation assay

SW48 cells ($1 \times 10^5$ cells/well) were seeded in a six-well plate and treated with aMan1 (25 μmol/L) or Pae1 (10 μmol/L) for 72 hours. After incubation, the adherent as well as floating cells were harvested. Genomic DNA was isolated by using the DNeasy Blood and Tissue Kit (Qiagen) including RNAse treatment. The genomic DNA (1 μg) was resolved on 2% Agarose gel containing ethidium bromide. The image was acquired using Gel Doc (Bio-Rad).

### Confocal microscopy

SW48 cells ($1 \times 10^5$ cells/well) were cultured in a six-well plate on glass cover slips in RPMI medium supplemented with FCS (10%). The cells were treated with aMan1 (25 μmol/L) or Pae1 (10 μmol/L) for 72 hours. Followed by incubation, the cells were fixed with paraformaldehyde (4%) and permeabilized with Triton X-100 (0.2%) in PBS for 10 minutes. After washing with PBS, the cells were blocked with 5% skim milk overnight and the nuclei were stained with DAPI for 1 hour at room temperature. After three washes with PBS, the cells were mounted on glass slides using DPX mounting medium and cured overnight. The images were captured using a Zeiss Apotome.

### Cell-cycle analysis

To investigate the effect of natural compounds on cell cycle, BjhTERT, HCT116, HT29, or SW48 cells ($1 \times 10^5$ cells/well) were seeded in 96-well plates and treated with either aMan (25 μmol/L),

aMan1 (25 μmol/L), Pae (300 μmol/L), or Pae1 (10 μmol/L) for 48 hours. Then the cells were incubated with EdU (10 μmol/L) for 20 minutes. After trypsinization, the cells were harvested, fixed with paraformaldehyde (4%) at room temperature for 15 minutes, and permeabilized with Triton X-100 (0.25%) for 10 minutes. The incorporated EdU was stained according to the manufacturer's protocol. After staining the cells with DAPI, the cells were analyzed by FACScanto.

### Western blotting

The HCT116_TP53_WT and KO cells were harvested and washed twice with 1× PBS and lysed in RIPA buffer (50 mmol/L Tris-HCl pH 8.0, 150 mmol/L NaCl, 1% NP-40, 0.5% DOC, 0.1% SDS) supplemented with antiproteases. Briefly, the cells were incubated with RIPA buffer on ice for 15 minutes and sonicated using the Bioruptor Next Gen (Diagenode) for five cycles (30 seconds ON and 30 seconds OFF) at a high-power setting. After centrifugation at 20,000 × *g* for 15 minutes at 4°C, the supernatant was collected and the total protein concentration was measured using Pierce BCA Protein Assay Kit (Thermo Fisher Scientific). The protein extracts were run on 4% to 20% Mini-PROTEAN TGX Stain-Free Gels (Bio-Rad) and transferred to nitrocellulose membranes (iBlot 2 Transfer Stacks; Thermo Fisher Scientific). After the transfer, the membranes were blocked in T-PBS (0.1% Tween 20 in PBS) supplemented with 5% milk for 2 hours at room temperature and then incubated with p53 WT-specific antibody (Sigma, A5316) and β-actin antibody (Santa Cruz Biotechnology, sc126) in T-PBS supplemented with 5% BSA overnight at 4°C. After incubation with primary antibody, the membranes were washed with T-PBS for 30 minutes at room temperature and then incubated with secondary antibody (HRP anti-mouse; 1:3,000) in T-PBS supplemented with 5% milk for 1 hour at room temperature. After incubation with the secondary antibody, the membranes were washed with T-PBS for 30 minutes at room temperature and then developed on an Amersham Imager 600 (GE Healthcare).

### Cytotoxicity and apoptosis analysis in human primary organoids

Human intestinal crypts were isolated from either tumor tissue or adjacent healthy tissue from the same patient and cultured as intestinal organoids according to the established protocol (27). Human intestinal organoids were seeded (100 organoids/well) in Labtec chamber slides containing 20 μL of Matrigel matrix and 300 μL of complete growth media for human organoids (27). After 24 hours of culturing, organoids were treated with various concentrations of either irinotecan (3, 6, and, 12 μmol/L), aMan (25, 50, and 100 μmol/L), aMan1 (25, 50, and 100 μmol/L), Pae (100, 200, and 400 μmol/L), or Pae1 (7.5, 15, and 30 μmol/L) for additional 48 hours. The images of organoids were captured with the use of Zeiss AxioCam MRc 5 (Carl Zeiss). Live and dead organoids were enumerated by their morphological appearance as described (28). For quantification of organoids cell death and apoptosis by flow cytometry, human intestinal organoids were seeded and treated with different concentrations of either irinotecan, aMan, aMan1, Pae, or Pae1. Following 48 hours of incubation, the organoids were harvested, washed with 1× PBS, and incubated with 200 μL of TrypleE mix (5 mmol/L $MgCl_2$, 10 μmol/L Y27632, 3.3 mmol/L EDTA, 5.5 mmol/L $CaCl_2$, and 5 μL DNAseI) for 10 minutes at 37°C. The organoids were disintegrated into single-cell suspension by vigorous pipetting 40 to 50 times. For apoptosis, the cells were incubated in 1x Annexin V conjugated to APC binding buffer (100 μL) for 20 minutes at room temperature. After washing, the cells were washed and resuspended in FACS buffer containing 2% FCS, DAPI, and inhibitor of apoptosis Y27632 (100 μmol/L). The samples were analyzed using FACScanto (BD Bioscience).

### RNA sequencing library preparation and data analysis

For RNA sequencing (RNA-seq) analysis, BjhTERT, SW48, HCT116_TP53_WT, and HCT116_TP53_KO cells were cultured in RPMI (GIBCO) medium supplemented with 10% FCS, 1 mmol/L sodium pyruvate (GIBCO) and 1× Glutamax (GIBCO). These cell lines ($1 \times 10^5$cells/well) were seeded in a six-well plate and on the next day were treated with either aMan1 (25 μmol/L) or Pae1 (10 μmol/L) for 48 hours. Total RNA was isolated with the use of QIAzol Lysis Reagent (Qiagen) followed by isopropanol precipitation. The concentration and integrity of RNA was estimated with the use of Fragment Analyzer (Agilent) and Qubit 3 Fluorometer (Thermo Fisher Scientific). Poly-A tail mRNA was enriched using magnetic beads. The first strand of cDNA was synthesized using Superscript III Reverse Transcriptase (Thermo Fisher Scientific), and the second strand was synthesized using the second strand master mix [TruSeq RNA Library Prep Kit V2 (Illumina)]. The synthesized DNA was cleaned up with the use of Agencourt AMPure XP Beads (Beckman Coulter). After end repair/dA-tailing, adaptors were ligated, and the library was further enriched with the use of TruSeq RNA Library Prep Kit V2 (Illumina). After determining the quality and concentration, the cDNA libraries were pooled and loaded (20 pmol/L) into the NextSeq500 Sequencer (Illumina) with the use of NextSeq 500/550 High Output Kit v2.5 (75 cycles).

Fastq files quality check was performed using FastQC v0.11.5. The fastq files were mapped to the hg19 genome using TopHat v2.1.0 (29) with the following parameters: bowtie1–no-coverage-search -a 5. The number of reads covered by each gene is calculated by HTSeq-Count 0.11.2 (30) with -s no -a 0 -t exon -m intersection-nonempty parameters and hg19 gencode.v19 annotation. Before further analysis, all of the rRNA genes were removed from the count data. For calculating differentially expressed genes (DEGs) and normalized count, DESeq2 R package v1.20.0 (31) was used with the default parameters. For Pearson correlation analysis, principal component analysis (PCA), gene set enrichment analysis (GSEA), and plotting the expression, the normalized count (DESeq2) was used. For PCA and Pearson correlation, only the genes with more than 10 counts in at least three samples and with the minimum interquartile range (IQR) of 1.5 in log2 transformed normalized counts were used for calculation. For functional and pathway analysis, DESeq2 differentially expression analysis (adjusted $P$ value < 0.01 and | log2 fold change | >= 1) results were uploaded in ingenuity pathway analysis (IPA; v45868156).

For gene set enrichment analysis, normalized counts (for each gene in all of the samples) were scaled using scale function in R (with center = TRUE, scale = TRUE parameters). The $z$-score was calculated by multiplying the scaled counts by +1 or −1, which shows the expected direction (+1 for upregulated genes and −1 for downregulated genes). For the three gene sets (cell cycle; DNA damage pathways; EGR/NF-κb pathways), +1 is used for all of the genes in the three gene sets, except CDKN2B, for which −1 is used. For EIF2 and mTOR signaling and protein ubiquitination pathway, the gene list and the directions are extracted from DEGs (adjusted $P$ value < 0.01 and | log2 fold change | ≥ 1) in comparison between SW48 cells treated with aMan1 versus DMSO. For the other three canonical pathways (Oxidative Phosphorylation, Sirtuin Signaling Pathway and Mitochondrial Dysfunction), DEGs of the comparison between SW48 cells treated with Pae1 versus DMSO are used. The average of $z$-scores were calculated for each group

(one value for each gene per group) and used for plotting and statistical test.

### Reverse transcription and qRT-PCR

SW48 cells ($1\times 10^6$/well) were seeded in a 24-well plate. On the following day, the cells were treated with Pae1 (10 μmol/L) for 24 hours. Following incubation, total RNA was isolated using QIAzol Lysis Reagent (Qiagen) as described previously, and the cDNA was synthesized using iScript cDNA Synthesis Kit (Bio-Rad, No. 1708891) according to the manufacturer's protocol. qPCR was performed for the genes CDKN2B, PCNA, E2F8, GADD45A, GADD45B, RASD1, NFKB1B, NFKB1E, and EGR2 using SYBR GreenER qPCR SuperMix (Invitrogen, No. 11761–500). The target gene expression was normalized to human β-actin. The reactions were performed in triplicates. The relative gene expression was determined using the relative $\Delta C_T$ method.

### Thermal proteome profile (TPP) assay

SW48 cells ($10 \times 10^5$/well) were seeded in a 15 $cm^2$ Petri plate. On the following day, the cells were treated with Pae1 (20 μmol/L) for 2 hours. After incubation, the adherent cells were trypsinized, harvested in 20-mL cold PBS, and centrifuged at 300 × *g* for 5 minutes at 4°C. The cells were washed once again with cold PBS 1×. After centrifugation, the cells were resuspended in cold PBS ($1 \times 10^6$ cells/100-μL PBS) and transferred to 0.2-mL PCR tubes (Axygen). After centrifugation at 300 × *g*, for 3 minutes at 4°C, PBS (90 μL) was removed. Then, the samples were incubated at various temperatures (37, 41, 44, 47, 50, 53, 56, 59, 63, 67°C) for 3 minutes in the T Professional Thermocycler (Analytik Jena GmbH). After bringing the samples to 25°C for 3 minutes, the samples were resuspended in RIPA Buffer (5 mmol/L TRIS-HCl pH 8.0, 150 mmol/L NaCl, 0.5% DOC, 1% NP-40, 0.1% SDS, and 1× protease inhibitor) and snap frozen in liquid nitrogen. After thawing, the samples were transferred to polycarbonate centrifuge tubes (Beckman Coulter, No. 343775) and centrifuged at 55.000 × *g* for 20 minutes at 4°C. Next, the supernatant was carefully transferred to the new PCR tubes. After adding lysis buffer (1% SDS, 100 mmol/L DTT, 100 mmol/L HEPES pH 8) to the supernatant of heat-treated samples, the samples were sonicated (Bioruptor Next Gen, Diagenode) for 10 cycles (30 seconds on/60 seconds off) at a high-power setting at 4°C and boiled at 95°C for 5 minutes. Cysteine residues were alkylated with 15 mmol/L iodoacetamide (30 minutes at room temperature in the dark). Proteins were precipitated with eight volumes of 100% acetone (overnight at −20°C) and washed twice with ice-cold 80% acetone. Pellets were resuspended in 1M guanidine chloride and 100 mmol/L HEPES pH 8 and digested with LysC (1:100 enzyme/protein; Lysyl Endopeptidase; Wako) for 4 hours at 37°C. Samples were treated with 1:2 of water and trypsin (1:100 enzyme/protein; trypsin, Promega) for 16 hours at 37°C. Following incubation, digested peptides were desalted using a Waters Oasis HLB μElution Plate following the manufacturer's instructions. Peptides were dried and resuspended in 0.1% formic acid and 5% acetonitrile for MS analysis. Peptides (20 μg) were used for TMT labeling (TMT10plex Isobaric Label Reagent, Thermo Fisher Scientific) and neutralized using 100 mmol/L HEPES (10% of sample volume). Each denaturing temperature of the TPP experiment was labeled with a different TMT label. TMT labelling was performed by adding 20-μg TMT (dissolved in DMSO). After 30 minutes of incubation at room temperature, a second portion of TMT reagent (20 μg) was added and incubated for another 30 minutes. Labelled peptides were cleaned using a Waters Oasis HLB μElution Plate prior to the pooling for the high pH fractionation. The high pH fractionation was performed as described previously (32). Offline high pH reverse phase fractionation was performed using an Agilent 1200 Infinity HPLC System equipped with a quaternary pump, degasser, variable wavelength UV detector (set to 254 nm), Peltier-cooled autosampler, and fraction collector (both set at 10°C for all samples). The column was a Gemini C18 column (3 m, 110 Å, 100 1.0 mm, Phenomenex) with a Gemini C18, 4, 2.0 mm SecurityGuard (Phenomenex) cartridge as a guard column. The solvent system consisted of 20 mmol/L ammonium formate (pH 10.0) as mobile phase (A) and 100% acetonitrile as mobile phase (B). The separation was accomplished at a mobile phase flow rate of 0.1 mL/min using the following linear gradient 1% B for 2 minutes, from 10% B to 40% B in 100 minutes, to 85% B in another minute, and held at 85% B for an additional 5 minutes. In total, 48 fractions were collected and pooled into 16 samples for MS analysis. Pooled fractions were dried and resuspended in 0.1% formic acid and 5% acetonitrile for MS analysis. Data were acquired as described previously (32) for SPS-MS3 acquisitions. In short, all acquisitions were performed on an Orbitrap Fusion Lumos mass spectrometer (Thermo Fisher Scientific) using the Proxeon nanospray source and coupled to a nanoAcquity UPLC (Waters) fitted with a trapping (nanoAcquity Symmetry C18, 5 μmol/L, 180 μmol/L × 20 mm) and an analytical column (nanoAcquity BEH C18, 1.7 μmol/L, 75 μmol/L x 250 mm). Solvent A was water, 0.1% formic acid and solvent B was acetonitrile, 0.1% formic acid. Full-scan MS spectra with mass range 375 to 1,500 *m*/*z* were acquired in profile mode in the Orbitrap with a resolution of 60,000 FWHM (at 200 *m*/*z*) using the quad isolation. The most intense ions from the full-scan MS were selected for MS2, using quadrupole isolation. HCD was performed in the ion trap with a normalized collision energy of 35%, with an intensity threshold of 5,000. For the MS3, the precursor selection window was set to the range 400 to 2,000 *m*/*z*, with an exclusion width of 18 *m*/*z* (high) and 5 *m*/*z*. The most intense fragments from the MS2 experiment were coisolated (using Synchronus Precursor Selection = 8) and fragmented by HCD (collision energy, 65%). MS3 spectra were acquired in the Orbitrap over the mass range 100 to 1,000 *m*/*z* and resolution set to 30,000. Mascot Daemon 2.5.1 (Matrix Science; ref. 33) was used to search the data via the IsobarQuant 1.1.0 Python package as described here (34). The database used consisted of the Swissprot human database (release 2016_01) with the reverse sequences added. The following settings were set for the search: fixed modifications were Carbamidomethyl (Cysteine) and TMT10plex (Lysine), whereas oxidation (methionine) and TMT10plex (N-term) were set as variable modifications. Maximal missed cleavage is 1 with the enzyme being trypsin, MS1 tolerance of 10 ppm, and MS2 tolerance of 0.5 Da. The output file from IsobarQuant was then further analyzed using the TPP package (35) from the Bioconductor R package in R-studio 3.6.3. The analyzeTPPTR function was used with the default settings and methods = "meltcurvefit." Only proteins with $P$ value <0.05 and a melting point difference >5 of the comparison from control 1 versus treatment 1 and were considered as targets. The melting temperature shifts for the selected targets were confirmed in an independent biological replicate.

### Statistical analysis

The statistical significance was calculated by using Graphpad Prism 5 (GraphPad Inc.). Differences with $P < 0.05$ were considered

significant, and the specific statistic used for each experiment is indicated in the figure legend.

### Data and materials availability

The DNA sequencing data have been deposited at the Geo Expression Omnibus database (GSE154755). The mass spectrometry data have been deposited at the ProteomXchange Consortium via the PRIDE partner repository. The data are available via ProteomXchange with identifier PXD024999. All other data are available from the authors upon reasonable request.

### Ethics approval and consent to participate

The work was approved by the ethics committee of the Jena University Hospital with the approval 5032–01/17 with the informed written consent from subjects and conducted in accordance with the Declaration of Helsinki.

### Consent for publication

All authors agreed to publication.

## Results

### Cell viability screening of aMan, Pae, and their derivatives in colorectal cancer cell lines

We chemically synthesized seven different derivatives of the natural products aMan and Pae (36) by adding functional groups (e.g., boronic acids) to improve the solubility, penetration, and selectivity toward cancer cells (**Fig. 1A–D**; Supplementary Figs. S1A–S1E). aMan low solubility is probably rendered by the two terpene groups. By using facile synthesis, aMan1 was prepared with an aldehyde group modification and xanthone core left intact, to improve solubility and to reduce the cytotoxicity. Although Pae exhibited good anti-inflammatory/oxidative activity and low cytotoxicity, it barely showed an anticancer effect. Moreover, its low solubility reduced its usefulness. To increase the solubility, the boronic acid group was used in one of the derivatives. More importantly, when attached to a sugar (e.g., a fructose), the boronic acid-fructose group can increase the selectivity of a compound concerning tumor cells. This idea is based on the design concept of boronophenylalanine-fructose (BPA-fructose), an agent applied in a clinical trials of boron neutron capture therapy (36–39). Even without the attachment of a sugar moiety, the strong affinity of a boronic acid group to the cell membrane can enhance the bioactivity of a compound that has interactions on membrane proteins, which are overexpressed more on tumor cells. In brief, we tried using a boronic acid group to improve solubility and, when needed, to attach a sugar moiety to "indirectly" increase the selectivity toward tumor cells. We performed a medium-throughput screening of all the derivatives on HCT116, HT29, and SW48 colon cancer cell lines to test whether these derivatives have an enhanced activity in selectively inhibiting cancer cell growth (**Fig. 1E–H**; Supplementary Figs. S1F—S1J).

We identified two derivates: 2-(3,6,8-trihydroxy-2-methoxy-7-(3-methylbut-2-en-1-yl)-9-oxo-9H-xanthen-1-yl) acetaldehyde that we named aMan1 and *e*-(4-(3-(2-hydroxy-4-methoxyphenyl)-3-oxo-prop-1-en-1-yl) phenyl) boronic acid that we named Pae1 (**Fig. 1**), which exhibited enhanced antiproliferative properties toward colon cancer cell lines compared with nontransformed cells (human noncancerous fibroblasts, BjhTERT). The parental compound aMan used at 40 μmol/L totally reduced the viability of colorectal cancer cells by 92% to 100% (**Fig. 1E** and **I**: the $IC_{50}$ values of aMan for BJhTERT, HCT116, HT29, and SW48 are 13.2, 13.8, 7.7, and 7.7 μmol/L, respectively) but also of human noncancerous fibroblasts (BjhTERT). The derivative compound aMan1 (at 40 μmol/L) decreased the viability all of all the three colon cancer cells by 95% to 99%; however, it was less toxic toward the human noncancerous fibroblasts (BjhTERT) and reduced the viability by only 30% (**Fig. 1F** and **I**: the $IC_{50}$ values of aMan1 for BJhTERT, HCT116, HT29, and SW48 are 57.4, 12.0, 14.1, and 14.0 μmol/L, respectively). Thus, aMan1 more specifically targets colon cancer cells and is less toxic to noncancerous fibroblasts. Pae showed cytotoxic effects on cancer cell lines, but required a high concentration (300 μmol/L) to reduce the viability of HCT116, HT29, and SW48 cells by ∼90% (**Fig. 1G** and **I**: the $IC_{50}$ values of Pae for BJhTERT, HCT116, HT29, and SW48 are 287.5, 188.6, 161.9, and 219.6 μmol/L, respectively). Pae1 required a consistently lower concentration (25 μmol/L) to reduce the viability of HCT116, HT29, and SW48 to 91%, 75%, and 86%, respectively (**Fig. 1H** and **I**: the $IC_{50}$ values of Pae1 for BJhTERT, HCT116, HT29, and SW48 are 38.1, 13.3, 15.7, and 11.1 μmol/L, respectively) and showed a higher cancer cell specificity compared with the parental compound. The other Pae derivatives showed no evident higher cancer-specific cytotoxicity than the parental compound (Supplementary Fig. S1). Therefore, Pae1 is more effective at a low concentration and has better selectivity toward the human colon cancer cell lines, compared with the parental compound.

### Characterization of the cytotoxic property of aMan, Pae, and their two enhanced derivatives in colorectal cancer cell lines

To better characterize the reduced viability of the colorectal cancer cell lines, we performed a flow cytometry (FACS) analysis with DAPI and Annexin V staining. DAPI reveals cell membrane permeability; therefore, it is an indicator of cellular death (**Fig. 2A** and **B**; Supplementary Fig. S2A). aMan and aMan1 induced cell death in all cancer cells lines (**Fig. 2A**). However, aMan1 induced significantly higher percentages of cell death in the cancer cell lines compared with the parental compound (**Fig. 2B**, top). aMan1 also showed strongly significant reduction of cellular death in BjhTERT cells when compared with the aMan treatment (**Fig. 2B**, top). Similarly, Pae1 induced significantly higher cell death in colon cancer cells at a very low concentration (25 μmol/L) compared with Pae, which induced cell death at a much higher concentration (300 μmol/L; Supplementary Fig. S2A, quantification in **Fig. 2B**, bottom). Also, Pae1 had a minimal cytotoxic effect on the BjhTERT fibroblast cells as compared with Pae (**Fig. 2B**, bottom).

To further understand whether the cellular death was mediated by an apoptotic program, we performed FACS analysis with Annexin V staining (**Fig. 2C** and **D**; Supplementary Fig. S2B). The derivative compounds showed a significantly higher induction of apoptosis, in all three colorectal cancer cell lines, whereas no apoptosis was observed in the BjhTERT cells (**Fig. 2C** and **D**; Supplementary Fig. S2B). Pae1 induced higher levels of apoptosis with a lower concentration compared with its parental compound (**Fig. 2D**, bottom; Supplementary Fig. S2B). Analysis of DNA fragmentation by agarose gel and DAPI fluorescence imaging confirmed the induction of apoptosis following aMan1 and Pae1 treatment (**Fig. 2E** and **F**). Thus, aMan1 and Pae1 displayed a significantly higher apoptosis-inducing activity than parental compounds in colorectal cancer cells but not in nontransformed cells. To investigate whether natural compounds inhibit apoptosis by blocking the activation of caspase cascade, we treated the colorectal cancer cell lines with natural compounds in the presence and absence of the pan caspase inhibitor Z-VAD-FMK. Addition of Z-VAD-FMK reduced aMan1- and Pae1-induced apoptosis in all three colorectal cancer cell lines (Supplementary Figs. S3A–S3C). Thus, both aMan1 and Pae1 induce apoptosis in a caspase-dependent pathway in colorectal cancer cell lines.

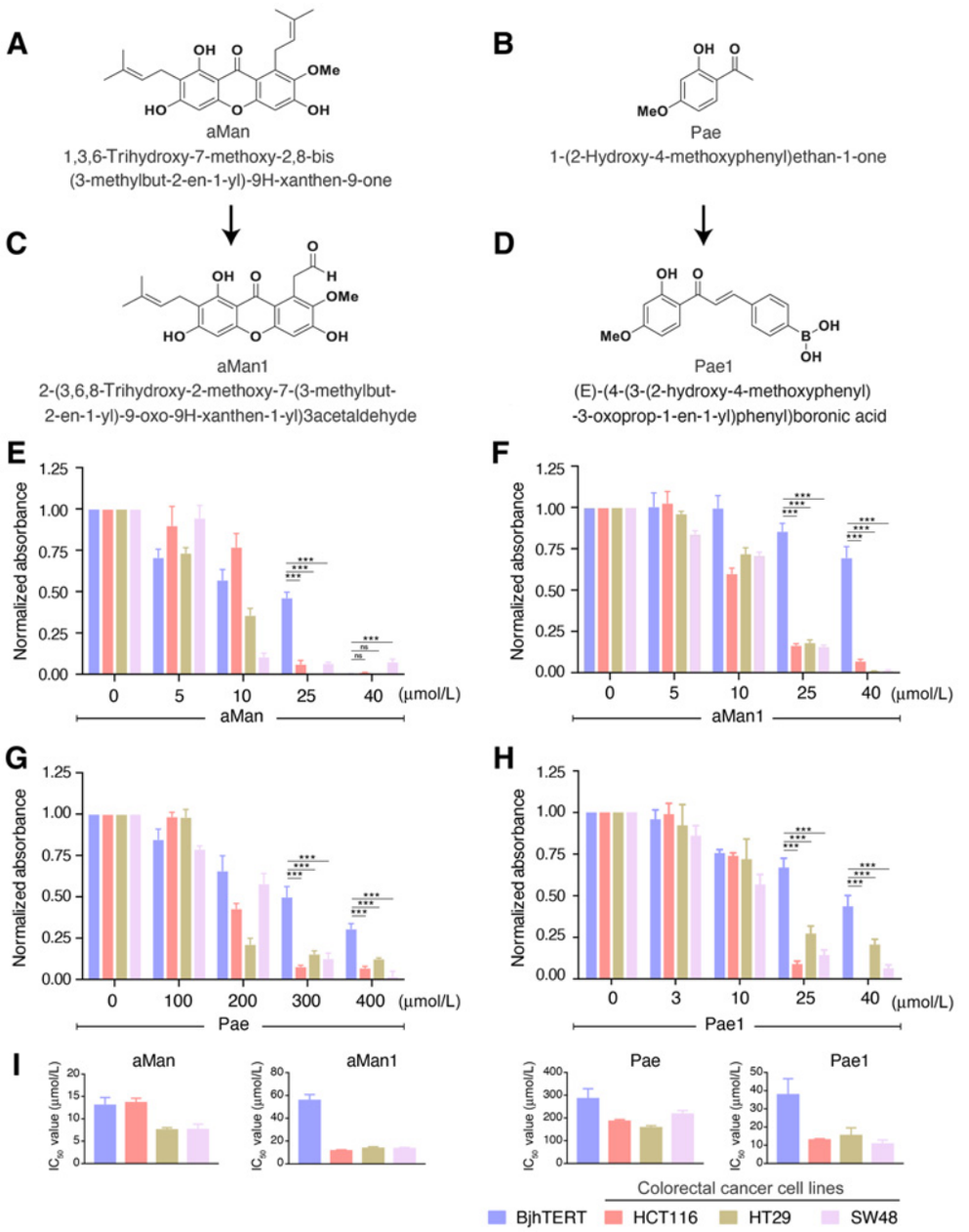


**Figure 1.**

Natural compounds inhibit the growth of human colon cancer cells. The chemical structure of aMan (**A**), Pae (**B**), aMan1 (**C**), and Pae1 (**D**). aMan (5, 10, 25, and 40 μmol/L; **E**), aMan1 (5, 10, 25, and 40 μmol/L; **F**), Pae (100, 200, 300, and 400 μmol/L; **G**), or Pae1 (3, 10, 25, and 40 μmol/L; **H**) were added to the BjhTERT, HCT116, HT29, and SW48 cell lines at the indicated concentrations for 72 hours. The viability of the cells was quantified by crystal violet assay. **I,** The $IC_{50}$ values of aMan, aMan1, Pae, and Pae1 for the indicated cell lines were calculated at 72 hours. **E, F, G, H**, and **I** indicate mean ± SD of three independent experiments. The statistical significance between two groups were analyzed by a two-tailed unpaired *t* test (*, $P \le 0.05$; **, $P \le 0.01$; ***, $P \le 0.001$).

### Characterization of the effect of aMan, Pae, and their two enhanced derivatives on the cell cycle in colorectal cancer cell lines

As an apoptotic program may be induced by the arrest of cells at specific cell-cycle phases, we analyzed the cell-cycle status by flow cytometry (**Fig. 3**). Both aMan and aMan1 arrested HCT116 cell lines in the $G_1$ phase of the cell cycle and HT29 and SW48 cell lines in the in the $G_2$–M phase of the cell cycle (**Fig. 3A**, quantification in **Fig. 3C**). However, in HT29 and SW48 cells, we also observed an increase of the overall DNA content indicating a potential appearance of polyploid cells perhaps due to events of endoreduplication suggesting that these two compounds may arrest cells in the $G_2$–M phase or rather increase the number of polyploid (≥4n) cells in an aberrant $G_1$ phase. Similarly, Pae and Pae-1 arrested HCT116 cell lines in the $G_1$ phase of the cell

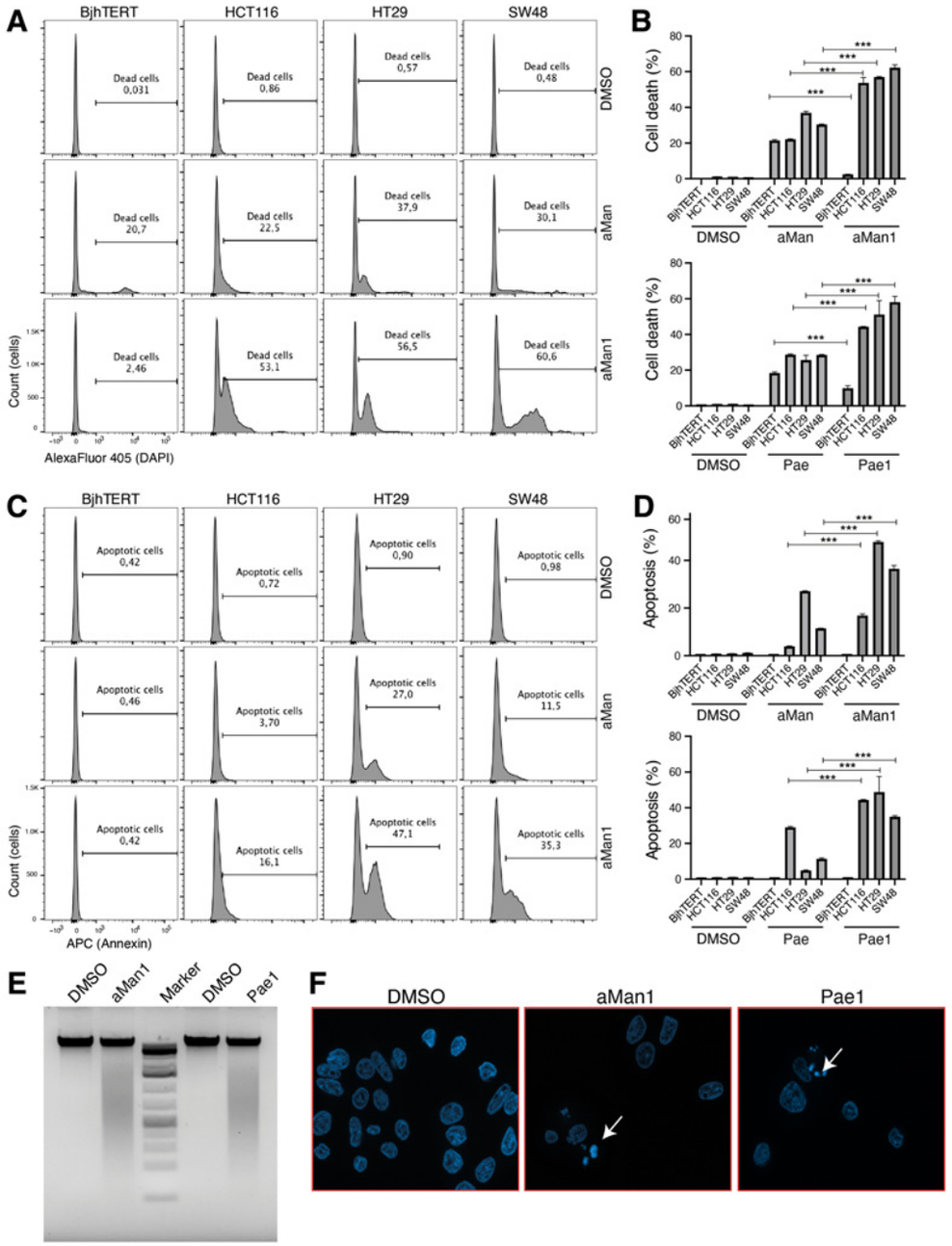


**Figure 2.**

Natural compounds induce cell death, apoptosis, and DNA fragmentation in colon cancer cell lines. **A,** aMan (25 μmol/L) or aMan1 (25 μmol/L) was added to BjhTERT, HCT116, HT29, and SW48 cell lines. After 48 hours, the cells were stained with DAPI, and the dead cells were quantified by flow cytometry. **B,** Quantification of the dead cells (in percentage) in the indicated different cell lines with the indicated treatments ($n = 3$). Pae and Pae1 were used at 300 and 10 μmol/L, respectively. **C,** Cells treated as in **A** were stained with Annexin V to quantify cell apoptosis by flow cytometry. **D,** Quantification of the apoptotic cells (in percentage) in the indicated different cell lines with the indicated treatments ($n = 3$). Pae was used at 300 μmol/L, and Pae1 was used at 10 μmol/L. **E, F,** aMan1 (25 μmol/L) and Pae1 (10 μmol/L) was incubated with SW48 cells. After 72 hours, chromatin degradation was visualized by agarose gel electrophoresis (**E**) and confocal microscopy (**F**; white arrows). **E** and **F** show representative view of a single experiment; however, the same result was observed in at least three independent replicates. **B** and **E** indicate mean ± SD of three independent experiments. The significance between the two groups was analyzed by a two-tailed unpaired *t* test (*, $P \leq 0.05$; **, $P \leq 0.01$; ***, $P \leq 0.001$).

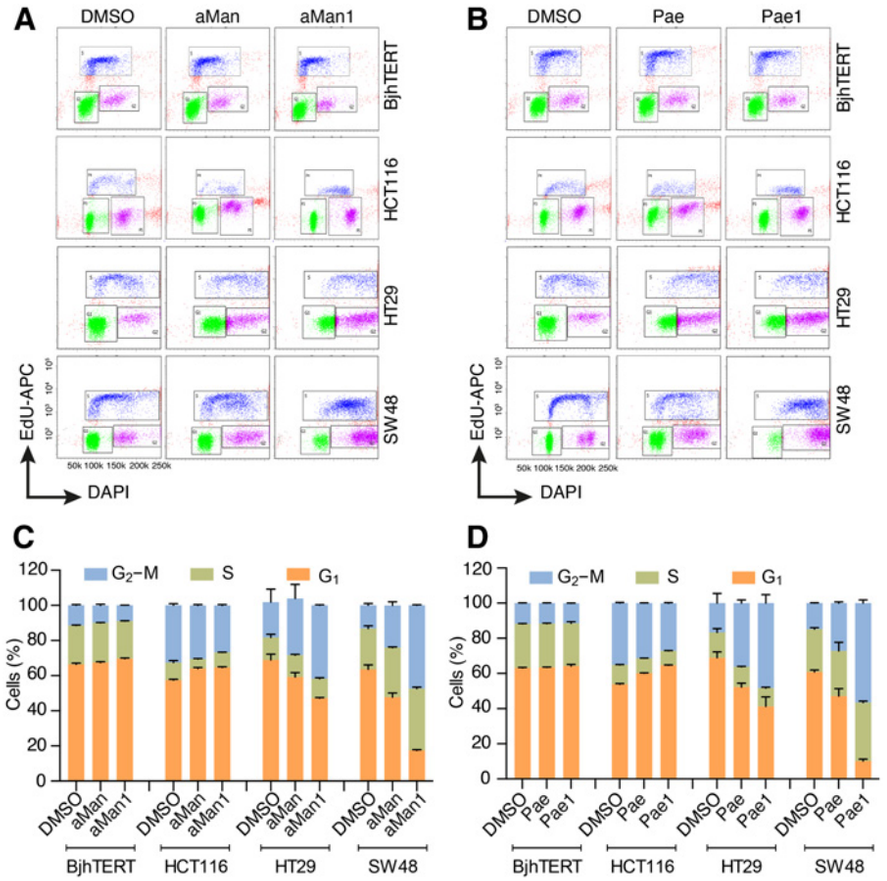


**Figure 3.**

Natural compounds arrest colon cancer cell lines at the $G_1$ or $G_2$–M stage of the cell cycle. **A,** aMan (25 μmol/L) or aMan1 (25 μmol/L), or (**C**) Pae (300 μmol/L), or Pae1 (10 μmol/L) was added to BjhTERT, HCT116, HT29, and SW48 cell lines for 48 hours. Then the cells were incubated with 5-ethynyl-2′-deoxyuridine (EdU), a nucleoside analogue of thymidine that incorporates into DNA during active DNA synthesis. After incubation, the cells were stained with azide conjugated to Alexa fluor and DAPI and were analyzed by FACS. **B–D,** Quantification of the distribution in each cell-cycle phase of cells treated with the indicated compounds. DMSO was used as control vehicle. **A** and **C** indicate single experiments from two independent replicates. **B** and **D** represent mean ± SD of two independent experiments.

cycle and HT29 and SW48 cell lines in the $G_2$–M (or the $G_1$ phase of polyploid cells) phase of the cell cycle (**Fig. 3B**, quantification in **Fig. 3D**). These results indicate that the derivative compounds arrest the cell cycle of colon cancer lines in a similar (slightly more powerful) manner with respect to their parental compounds suggesting similar mechanisms of action and that the response to the treatment can be different in different colorectal cancer cells.

### Characterization of the transcriptional response following the aMan1 and Pae1 treatment of the SW48 colorectal cancer cell line

To better characterize the molecular phenotype, we performed transcriptomic analysis (RNA-seq) of the SW48 cells treated with aMan1 or Pae1 for 24 hours. Hierarchical clustering heat-map of Pearson correlation of whole-transcriptomes showed that the Pae1- or aMan1-treated SW48 cells clustered separately with respect to the untreated cells (two replicates for each condition), in contrast to the treated and untreated BjhTERT cells which clustered together (**Fig. 4A**). PCA analysis of the datasets further confirmed that BjhTERT were not transcriptionally affected by aMan1 treatment and slightly responded to the Pae1 treatment (Supplementary Figs. S4A and S4B). These two analyses strongly suggest that the Pae1 or aMan1 treatments induced a more massive transcriptional response in cancer cells than in nontransformed cells. This observation is supported by the number of significantly DEG following treatments that was about 10 times higher in SW48 cells than in BjhTERTcells (**Fig. 4B**).

We performed gene ontology (GO) analysis of the DEGs in cancer cells and found that both aMan1 and Pae1 treatments induced transcriptional regulation of genes involved in cell-cycle regulation and DNA damage response confirming the results of the experiments described in **Figs. 2** and **3** (**Fig. 4C** and **D**). In particular, proliferation-associated genes (e.g., CCND1, CCNA2, PCNA) were strongly downregulated, whereas cell-cycle inhibitors like CDKN2B were upregulated in cancer cells after treatments (**Fig. 4E** and **F**, left). Pae1, but not aMan1 slightly affected these genes also in the BjhTERT (**Fig. 4E** and **F**, left). Remarkably, cancer cells treated with both the compounds showed a strong upregulation of genes involved in DNA damage response and in the EGR/NF-κB pathways (**Fig. 4E** and **F**, middle and right), suggesting that NF-κB, EGR, and GADD45 genes may be sequentially activated upon DNA damage following treatment with the compounds (40). Interestingly, this pathway is only activated in cancer cells, but not in BjhTERT cells. GO analysis showed enrichment of signaling pathways involving genes that might be regulated in metabolic stress response. In particular, EI2F signaling, mTOR signaling, and protein ubiquitination pathways may indicate an endoplasmic reticulum (ER) stress in cells treated with aMan1, whereas oxidative phosphorylation, sirtuin signaling, and mitochondrial dysfunction pathways suggest the occurrence of a mitochondrial stress response in cells treated with Pae1 (Supplementary Figs. S4C and S4D). Geneset enrichment analysis of these pathways showed that ER stress-response–related genes were specifically enriched in SW48 cells after aMan1 treatment,

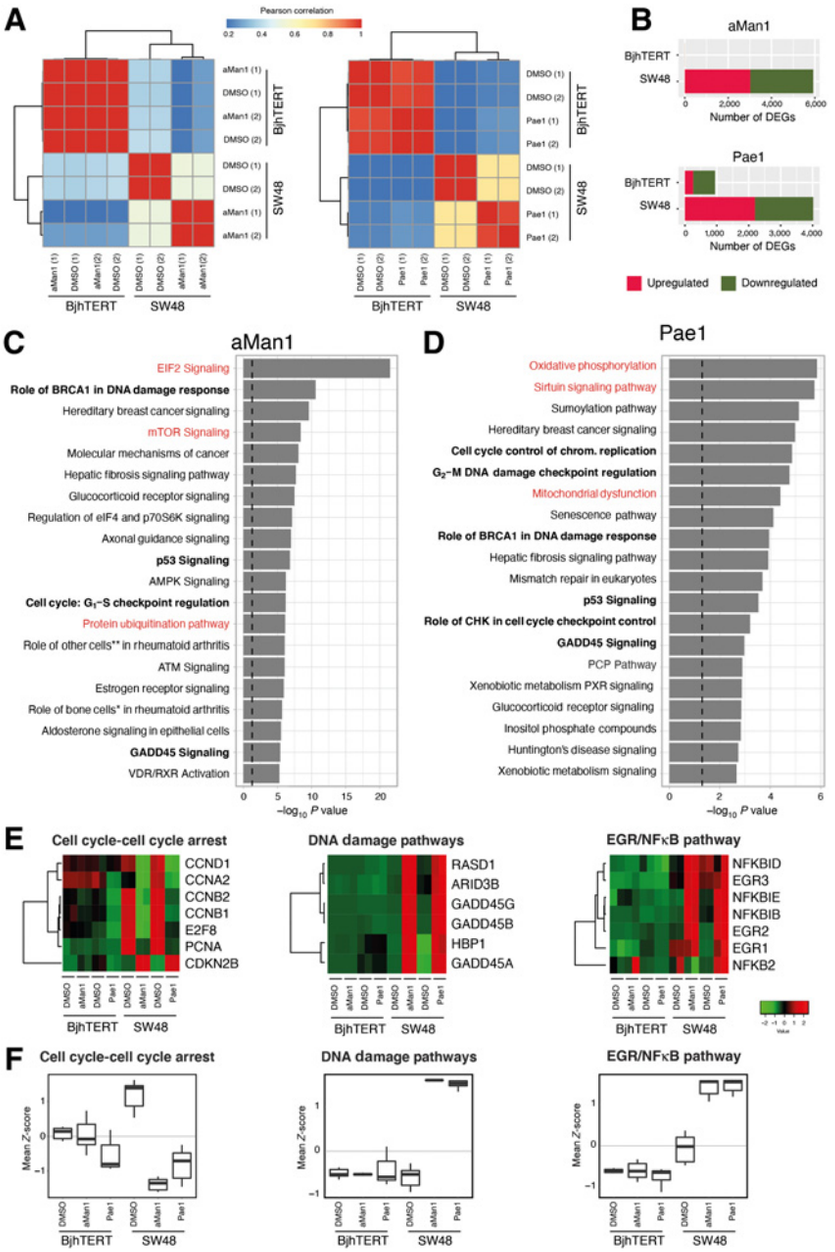


**Figure 4.**

aMan1 and Pae1 induce DEGs in SW48 colorectal cancer cell lines. **A,** Person correlation and hierarchical clustering of transcriptional profiles (RNA-seq) of aMan1 (25 μmol/L), Pae1 (10 μmol/L), or DMSO treated (24 hours) SW48 or BjhTERT cells. **B,** Number of DEGs (adjusted *P* value <0.05 and |log2 fold change|≥1) upon aMan1 or Pae1 treatment in the indicated cell lines. **C–D,** Top 20 significantly enriched canonical pathways (IPA software) in DEGs (adjusted *P* value <0.01 and |log2 fold change|≥1) found in SW48 cells upon aMan1 (**C**), or Pae1 (**D**) treatment. The *x*-axis shows the −log10 of enrichment *P* value. The dashed line shows the statistical significance threshold (−log10 0.05 = 1.3). **, Macrophages, fibroblasts, and endothelial cells; *, Osteoblasts, osteoclasts, and chondrocytes. **E,** Hierarchical clustering and heat map of three different gene sets upon aMan1 or Pae1 treatment in the indicated cell lines. **F,** Gene set enrichment analysis of the indicated gene sets (from **E**) in the specified conditions.

whereas mitochondria stress-response–associated pathways were specifically enriched in cancer cells treated with Pae1 (Supplementary Fig. S4D). Furthermore, the expression levels of selected genes from RNA-seq data were further validated by RT-qPCR (Supplementary Fig. S5).

### Cytotoxic activity of aMan1 and Pae1 and cellular stress response following treatment is largely maintained in TP53-deficient colorectal cancer cells

Since we found enrichment of the TP53 signaling pathway (**Fig. 4C** and **D**), and it has been previously reported that aMan induces apoptosis in a TP53-dependent manner (9), we questioned if the TP53 proficiency was a necessary condition to preserve the cytotoxicity and cancer selectivity of the two derivative compounds. Therefore, we tested aMan1 and Pae1 on HCT116 cells KO for TP53 (Supplementary Fig. S6A). HCT116_TP53_KO cells showed decreased apoptosis following aMan1 and Pae1 treatment (from ∼41% to ∼33% and ∼44 to ∼27%, respectively, with respect to the HCT116 cells WT for TP53), suggesting that TP53 is important in inducing aMan1-mediated apoptosis but also that additional TP53-independent pathways are taking place to carry out this function (**Fig. 5A** and **B**). Additional MTT assays showed that cytoxicity occurs both in HCT116 cells WT and KO for TP53 (**Fig. 5C**). RNA-seq analysis of the HCT116 cells treated with aMan1 and Pae1 showed that although transcriptionally different, HCT116WT or KO for TP53 responded similarly to the two derivative compounds (Supplementary Fig. S6B). HCT116_TP53_WT cells have a higher basal expression of the TP53 gene and its known targets P21 and $P15^{INK4b}$ as well

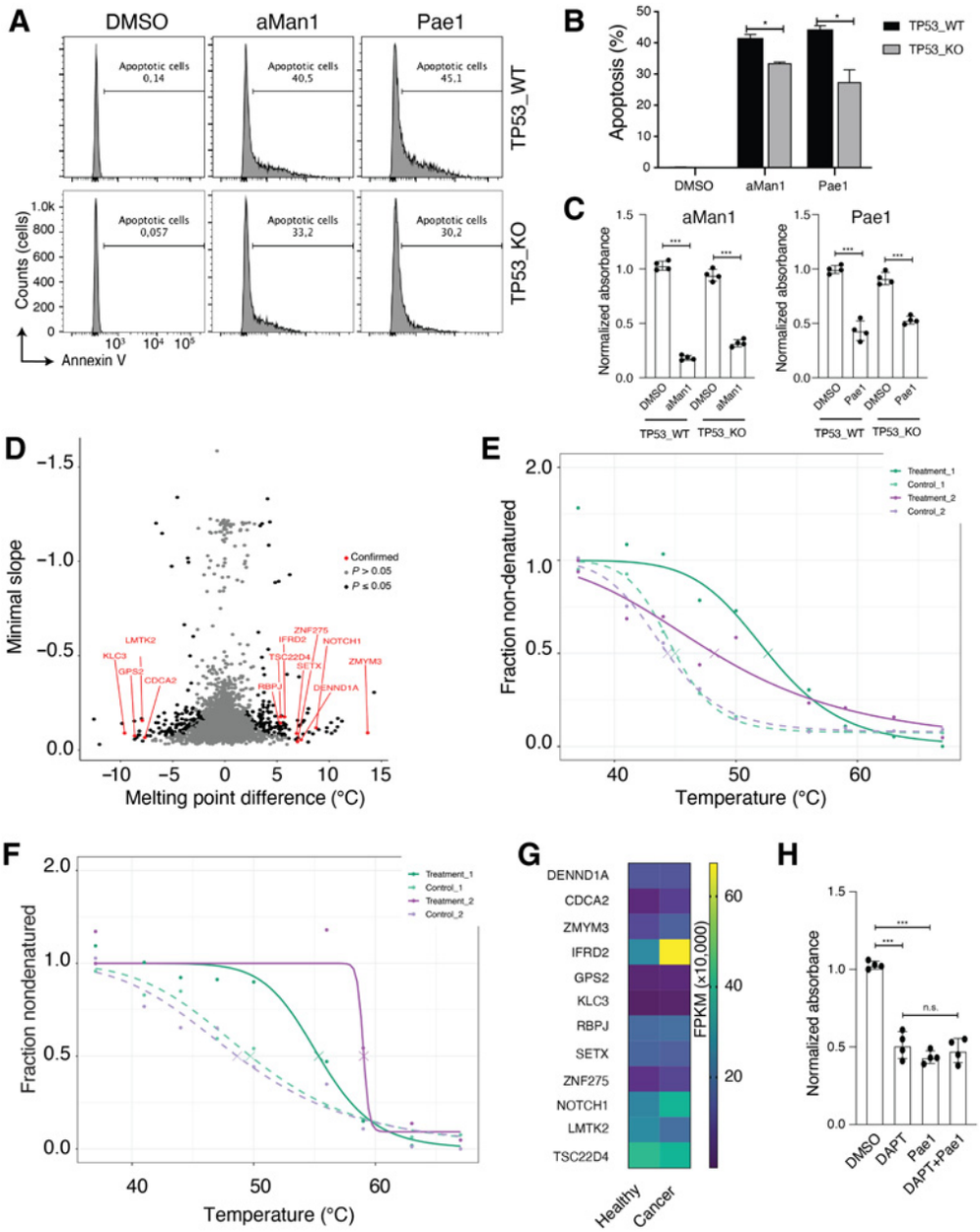


**Figure 5.**

aMan1 and Pae1 induce higher percentage of apoptosis in HCT116 wild-type cell than TP53 knockout cells. **A,** aMan1 (25 μmol/L) or and Pae1 (10 μmol/L) was added to HCT116 wild-type and TP53 knockout cells. After 48 hours, the cells were stained with Annexin V and analyzed by flow cytometry. **B,** Quantification of apoptosis (in percentage) in WT and KO cell lines with the indicated treatments. **C,** MTT assay in WT and KO cell lines with the indicated treatments. **D,** Melting point differences between Pae1 treated versus DMSO control treated in SW48 cells. **E** and **F,** Melting curves of NOTCH1 (**D**) and IFRD2 (**E**). **G,** The FPKM (fragment per kilo base pair transcript per million sequenced reads) of human normal and colorectal cancer tumor samples were downloaded from The Cancer Genome Atlas (TCGA) database. **H,** MTT assay in SW48 cells with the indicated treatments. The *P* value is calculated using two-tailed unpaired *t* test. **B, C,** and **H** shows mean ± SD of at least three independent experiments (*, $P \le 0.05$; **, $P \le 0.01$; and ***, $P \le 0.001$).

as transcriptional upregulation of these genes after treatment in contrast to the HCT116_TP53_KO cells (Supplementary Fig. S6C). However, both the HCT116 cell lines have a downregulation of cell-cycle related genes and upregulation of genes belonging to the DNA damage and EGR/NF-κB signaling pathways as previously observed in the SW48 CRC cell line (Supplementary Fig. S6D). Remarkably, ER stress-response pathways were again observed only following aMan1 treatment (in both HCT116_TP53_WT and HCT116_TP53_KO cells; Supplementary Fig. S7A). Mitochondrial stress-response pathways were observed in both the cell lines and following the treatments with both aMan1 and Pae1 (Supplementary Fig. S7B). These results suggest that aMan1 or

Pae1 may induce a cellular metabolic stress involving ER or mitochondria that can lead to DNA damage and activation of both TP53-dependent and -independent cell-cycle arrest and induction of the apoptotic programs. One candidate pathway involved in the DNA damage response is the NF-κB/EGR/GADD45 pathways that has already been shown to work in a TP53-independent manner (41). Very importantly, neither the metabolic stress nor the potential consequent DNA damage and DNA damage response is shown in noncancerous BjhTERT cells. These analyses revealed the importance of the cancer mutational profile in modulating the anticancer activity of the aMan1 and Pae1 treatment and also provide evidence that these compound derivatives may be used in P53-deficient tumors.

Taken together, these results show that aMan1 and Pae1 provoke a strong transcriptional response in colorectal cancer cells (not present in nontransformed cells), involving metabolic stress and DNA damage-response signaling pathways, ultimately leading to the cell-cycle arrest and induction of apoptotic programs.

To identify target proteins capable of interacting with the natural compound, we performed TPP assay in SW48 cells treated with Pae1. Pae1 targets were identified on the basis of the induced shift in melting temperature (34). Compared with DMSO treatment, Pae1 induced significant shifts in melting temperature of 12 proteins (**Fig. 5D**). Interestingly, Pae1 induced a thermal shift in NOTCH1, which is involved in various cancers (**Fig. 5E**) and IFRD2 (at this time, the function of IFRD2 is still unclear) (**Fig. 5F**). These two genes are transcriptionally highly expressed and upregulated in colon cancers (**Fig. 5G**), suggesting that they may represent ideal cancer-specific targets for chemotherapeutic drugs. By using a NOTCH1 signaling inhibitor (DAPT), we assessed the relationship between NOTCH1 signaling and treatment with Pae1. Inhibition of NOTCH1 led to reduction in cell viability, but no further reduction in cell viability was observed when the treatment was combined with Pae1 (**Fig. 5H**), suggesting that NOTCH1 signaling may be required for the action of Pae1 compound.

### Characterization of the cytotoxic property of aMan, Pae, and their two derivatives in human primary intestinal organoids

To investigate the effect of natural compounds on human intestinal organoids, we have isolated the crypts from colorectal tumor tissue as well as normal colonic epithelium from biopsies (surgery leftover) of the same patient. This procedure allows side-by-side organoid culturing, testing and screening of drugs for their anticancer activity, and assessing the adverse toxic side effects on normal tissue. To assess whether natural compounds induce apoptosis selectively in tumor cells, human colon cancer organoids and healthy tissue organoids from the same patient were plated in equal number, and organoids were treated with various concentrations of aMan, aMan1, Pae or Pae1 for 48 hours (**Fig. 6A**). We used irinotecan (a camptothecin analog) that is currently used as a chemotherapeutic drug for colorectal cancers and DMSO as a positive and negative control, respectively. At the minimal concentration required to induce cellular death in all of the cancer organoids, irinotecan, aMan, and Pae were also inducing cellular death in ∼50% of the normal healthy colon organoids derived from the tumor surrounding healthy tissue (**Fig. 6A**, quantification in **B**). Importantly and reflecting the cell viability assays in the colorectal cancer cell lines, aMan1 and Pae1 did not show any cytotoxic effect in the healthy colon tissue cultures (**Fig. 6A**, quantification in **B**). Furthermore, the cell death induced by the natural compound was analyzed with the use of flow cytometry (Supplementary Figs. S8A and S8B). Irinotecan, Man and Pae compounds induced cell death in cancer organoids and also healthy colon organoids. However, Man1 and Pae1 induced cell death only in cancer organoids without inducing any cytotoxicity in healthy organoids (Supplementary **Fig. 6**).

In cancer organoids, aMan1 and Pae1 induced apoptosis (**Fig. 6C** and **D**), but no apoptosis was observed in healthy organoids. Therefore, aMan1 and Pae1 showed a higher induction of cell death and apoptosis in cancer organoids but not in healthy organoids.

Taken together, these results confirm that our observations from the two-dimensional colorectal cancer cell lines are also applicable in *ex vivo* human organoids, strongly suggesting that the two derivatives of the natural compounds aMan and Pae have a strong selectivity in targeting only cancer cells and thus promoting them as potential novel promising compounds for the treatment of patients with colorectal cancer.

## Discussion

Natural compounds represent a wide variety of relatively cheap and suitable molecules that often have been used for various therapeutic aims since ancient times; for example, aMan and Pae derived from plants are used in traditional Chinese medicine. However, these two compounds, although they showed mild anticancer properties, never reached a clinical phase because of some physical and chemical features (e.g., low solubility and low membrane permeability) that make them unsuitable as drugs. In this study, we tested some chemical derivatives of these two compounds aimed to enhance their solubility, cell membrane penetration, and/or cancer selectivity. We screened for those derivatives that performed better than the parental compounds, with particular focus on two important features (enhanced cytotoxicity and cancer selectivity) and two of them (aMan1 and Pae1) were selected for further characterization. Pae1 showed higher cytotoxicity at a lower concentration than the Pae parental compound as previously reported in colon cancer cells (18, 24, 42). The overall increased cytotoxicity of Pae may be due to its transformation into a chalcone, but we think that the selectivity toward tumor cells was greater due to the boronic acid group allowing lower dosages. aMan was previously reported to induce cytotoxicity in colorectal cancer cell lines in a comparable manner as currently used chemotherapeutics (43); however, no data were provided for nontransformed cells. Our data show that aMan has cytotoxic effects also on noncancerous cells, suggesting that hypothetical treatment with this compound may generate a patient's detrimental side effects. aMan1 showed less cytotoxicity especially on noncancerous cells, indicating that it may be possible to find a drug concentration window in which the drug has cytotoxic effects on cancer cells, but no side effects in patients. RNA-seq analysis indicated that the two derivative compounds cause metabolic stress in the cells (probably by inducing ER or mitochondria stress) that further activates DNA damage response leading to the cell-cycle arrest and apoptosis of cancer cells through a CASPASE-dependent mechanism similarly to that previously observed for the parental compounds (24, 42, 44). We also showed that aMan1 and Pae1 have similar activity (slightly lower) in cancer cell lines deficient for TP53, one of the major players in mediating cell apoptosis probably through the P53-independent signalling of the NF-κB/EGR/GADD45 pathway (11). Finally, we showed that aMan1 and Pae1 are able to kill organoids from colon cancer and do not show any toxic effect on colon organoids from healthy tissue. Therefore, they

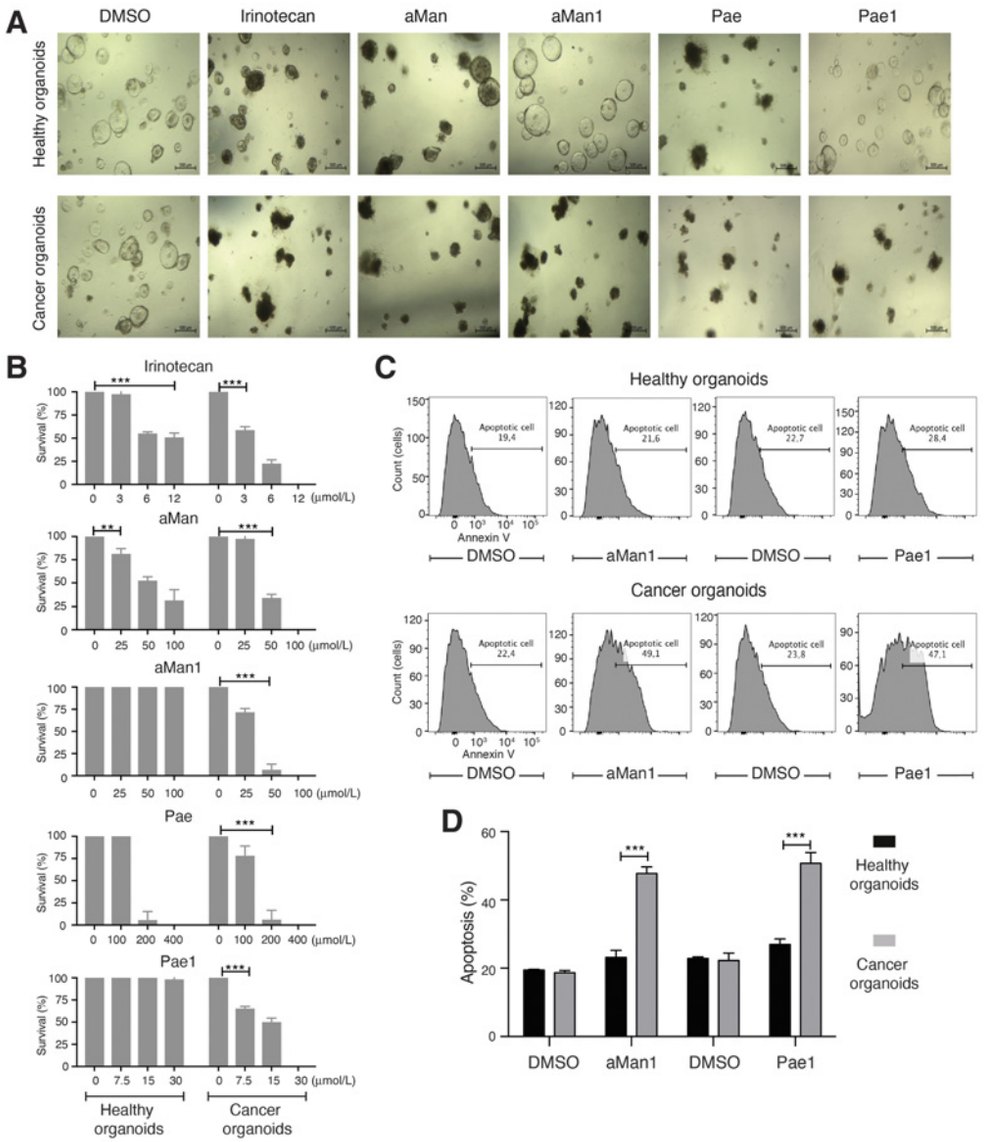


**Figure 6.**

aMan1 and Pae1 induce apoptosis is cell death in human organoids derived from colorectal cancer, but not from healthy colon tissue. **A,** Representative picture of organoids derived from healthy colon epithelium (top) or cancer tissue (bottom) of the same patient treated with irinotecan (12 μmol/L), aMan (100 μmol/L), aMan1 (100 μmol/L), Pae (400 μmol/L), or Pae1 (30 μmol/L) for 48 hours. **B,** Quantification of the survival of organoids (in percentage) derived from healthy or tumor tissue treated with natural compounds at the indicated concentrations. The statistical significance was analyzed by using Dunnett multiple comparisons test (*, adj $P \le 0.05$; **, adj $P \le 0.01$; ***, adj $P \le 0.001$; and ****, adj $P \le 0.0001$). **C,** Natural compound–induced apoptosis was determined by flow cytometry Annexin V staining. **D,** Quantification of the apoptotic cells (in percentage) in healthy and tumor organoid cells treated with aMan1 (100 μmol/L) and Pae1 (300 μmol/L; $n = 3$). The statistical significance was analyzed by using a two-tailed unpaired *t* test (*, $P \le 0.05$; **, $P \le 0.01$; and ***, $P \le 0.001$). **A** and **C** show single experiments out of three independent replicates. **B** and **D** show mean ± SD of three independent experiments.

performed much better than the parental compounds as well as some currently used chemotherapeutic drugs like irinotecan. We tested aMan1 and Pae1 in colon cancer cell lines and in colon cancer organoids. However, assessment of these two compounds in other cancers should be performed because they could also show selective anticancer properties in other types of cancer, especially solid epithelial tumors.

Taken together, our data promote these two natural compound derivatives as potential promising anticancer agents and provide breakthrough, novel findings on functional groups that can be used in drug development. In addition, these results point out that the selective targeting of cancer cells can be reached, and it is a reasonable aim during drug design and lead compound optimization. We think that identification of cancer-specific molecules and pathways is one of

the most desirable targets in cancer research, and our data can open new horizons in this direction.

## Authors' Disclosures

No disclosures were reported.

## Authors' Contributions

**F. Neri:** Conceptualization, data curation, supervision, funding acquisition, investigation, writing–original draft, project administration, writing–review and editing. **S. Nunna:** Data curation, validation, investigation, writing–original draft, writing–review and editing. **Y-P. Huang:** Data curation, investigation. **M. Rasa:** Data curation, formal analysis, investigation. **A. Krepelova:** Data curation, supervision, validation, investigation, writing–review and editing. **F. Annunziata:** Data curation, investigation. **L. Adam:** Data curation, investigation. **S. Käppel:** Data curation, investigation. **M-H. Hsu:** Conceptualization, data curation, supervision, writing–review and editing.

## Acknowledgments

The authors are grateful for the support by core facilities FACS, Proteomics, Sequencing and Microscopy at the Leibniz Institute on Aging–Fritz Lipmann Institute. HCT116_TP53_KO cells were kindly provided by Prof. Bert Vogelstein, and BjhTERT cells were provided by Dr. Helmut Pospiech. This work was supported by funding from the Fritz-Lipmann-Institute (FLI), Alexander von Humboldt and Fritz-Thyssen foundations.

The costs of publication of this article were defrayed in part by the payment of page charges. This article must therefore be hereby marked *advertisement* in accordance with 18 U.S.C. Section 1734 solely to indicate this fact.

Received September 10, 2020; revised April 22, 2021; accepted November 3, 2021; published first November 17, 2021.

## References

1. Araghi M, Soerjomataram I, Jenkins M, Brierley J, Morris E, Bray F, et al. Global trends in colorectal cancer mortality: projections to the year 2035. Int J Cancer 2019;144:2992–3000.
2. Hughes LAE, Simons C, van den Brandt PA, van Engeland M, Weijenberg MP. Lifestyle, diet, and colorectal cancer risk according to (Epi)genetic instability: current evidence and future directions of molecular pathological epidemiology. Curr Colorectal Cancer Rep 2017;13:455–69.
3. Coppedè F, Lopomo A, Spisni R, Migliore L. Genetic and epigenetic biomarkers for diagnosis, prognosis and treatment of colorectal cancer. World J Gastroenterol 2014;20:943–56.
4. Golshani G, Zhang Y. Advances in immunotherapy for colorectal cancer: a review. Therap Adv Gastroenterol 2020;13:1756284820917527.
5. Xie YH, Chen YX, Fang JY. Comprehensive review of targeted therapy for colorectal cancer. Signal Transduct Target Ther 2020;5:22.
6. Devlin EJ, Denson LA, Whitford HS. Cancer treatment side effects: a meta-analysis of the relationship between response expectancies and experience. J Pain Symptom Manage 2017;54:245–58.
7. Tofthagen C. Surviving chemotherapy for colon cancer and living with the consequences. J Palliat Med 2010;13:1389–91.
8. Whitford HS, Olver IN. When expectations predict experience: the influence of psychological factors on chemotherapy toxicities. J Pain Symptom Manage 2012; 43:1036–50.
9. Lee JH, Khor TO, Shu L, Su ZY, Fuentes F, Kong AN. Dietary phytochemicals and cancer prevention: Nrf2 signaling, epigenetics, and cell death mechanisms in blocking cancer initiation and progression. Pharmacol Ther 2013; 137:153–71.
10. Newman DJ, Cragg GM. Natural products as sources of new drugs over the 30 years from 1981 to 2010. J Nat Prod 2012;75:311–35.
11. Zaidi SF, Ahmed K, Saeed SA, Khan U, Sugiyama T. Can diet modulate helicobacter pylori-associated gastric pathogenesis? an evidence-based analysis. Nutr Cancer 2017;69:979–89.
12. Abotaleb M, Samuel SM, Varghese E, Varghese S, Kubatka P, Liskova A, et al. Flavonoids in cancer and apoptosis. Cancers (Basel) 2018;11.
13. Saha S, Sadhukhan P, Sil PC. Mangiferin: a xanthonoid with multipotent anti-inflammatory potential. Biofactors 2016;42:459–74.
14. Shan T, Ma Q, Guo K, Liu J, Li W, Wang F, et al. Xanthones from mangosteen extracts as natural chemopreventive agents: potential anticancer drugs. Curr Mol Med 2011;11:666–77.
15. Phan TKT, Shahbazzadeh F, Pham TTH, Kihara T. Alpha-mangostin inhibits the migration and invasion of A549 lung cancer cells. PeerJ 2018;6:e5027.
16. Korm S, Jeong H-C, Kwon O-S, Park J-R, Cho H, Kim Y-M, et al. α-Mangostin induces G1 cell cycle arrest in HCT116 cells through p38MAPK-p16INK4a pathway. RSC Adv 2015;5:34752–60.
17. Martinez-Abundis E, Garcia N, Correa F, Hernandez-Resendiz S, Pedraza-Chaverri J, Zazueta C. Effects of alpha-mangostin on mitochondrial energetic metabolism. Mitochondrion 2010;10:151–7.
18. Xing G, Zhang Z, Liu J, Hu H, Sugiura N. Antitumor effect of extracts from moutan cortex on DLD-1 human colon cancer cells in vitro. Mol Med Rep 2010; 3:57–61.
19. Zhang KJ, Gu QL, Yang K, Ming XJ, Wang JX. Anticarcinogenic effects of alpha-mangostin: a review. Planta Med 2017;83:188–202.
20. Cai Y, Luo Q, Sun M, Corke H. Antioxidant activity and phenolic compounds of 112 traditional Chinese medicinal plants associated with anticancer. Life Sci 2004;74:2157–84.
21. Li N, Fan LL, Sun GP, Wan XA, Wang ZG, Wu Q, et al. Paeonol inhibits tumor growth in gastric cancer *in vitro* and *in vivo*. World J Gastroenterol 2010;16: 4483–90.
22. Lyu ZK, Li CL, Jin Y, Liu YZ, Zhang X, Zhang F, et al. Paeonol exerts potential activities to inhibit the growth, migration and invasion of human gastric cancer BGC823 cells via downregulating MMP2 and MMP9. Mol Med Rep 2017;16: 7513–9.
23. Bao MH, Zhang YW, Zhou HH. Paeonol suppresses oxidized low-density lipoprotein induced endothelial cell apoptosis via activation of LOX-1/ p38MAPK/NF-kappaB pathway. J Ethnopharmacol 2013;146:543–51.
24. Li M, Tan SY, Wang XF. Paeonol exerts an anticancer effect on human colorectal cancer cells through inhibition of PGE (2) synthesis and COX-2 expression. Oncol Rep 2014;32:2845–53.
25. Bunz F, Dutriaux A, Lengauer C, Waldman T, Zhou S, Brown JP, et al. Requirement for p53 and p21 to sustain G2 arrest after DNA damage. Science 1998;282:1497–501.
26. Bioquest A. 2021, April 15.
27. Sato T, Stange DE, Ferrante M, Vries RG, Van Es JH, Van den Brink S, et al. Long-term expansion of epithelial organoids from human colon, adenoma, adenocarcinoma, and Barrett's epithelium. Gastroenterology 2011;141:1762–72.
28. Grabinger T, Luks L, Kostadinova F, Zimberlin C, Medema JP, Leist M, et al. Ex vivo culture of intestinal crypt organoids as a model system for assessing cell death induction in intestinal epithelial cells and enteropathy. Cell Death Dis 2014;5:e1228.
29. Trapnell C, Roberts A, Goff L, Pertea G, Kim D, Kelley DR, et al. Differential gene and transcript expression analysis of RNA-seq experiments with TopHat and Cufflinks. Nat Protoc 2012;7:562–78.
30. Anders S, Pyl PT, Huber W. HTSeq—a Python framework to work with high-throughput sequencing data. Bioinformatics 2015;31:166–9.
31. Love MI, Huber W, Anders S. Moderated estimation of fold change and dispersion for RNA-seq data with DESeq2. Genome Biol 2014;15:550.
32. Buczak K, Kirkpatrick JM, Truckenmueller F, Santinha D, Ferreira L, Roessler S, et al. Spatially resolved analysis of FFPE tissue proteomes by quantitative mass spectrometry. Nat Protoc 2020;15:2956–79.
33. Perkins DN, Pappin DJ, Creasy DM, Cottrell JS. Probability-based protein identification by searching sequence databases using mass spectrometry data. Electrophoresis 1999;20:3551–67.
34. Franken H, Mathieson T, Childs D, Sweetman GM, Werner T, Togel I, et al. Thermal proteome profiling for unbiased identification of direct and indirect drug targets using multiplexed quantitative mass spectrometry. Nat Protoc 2015; 10:1567–93.
35. Hertel NT, Jensen PB, Jensen TS. [Treatment of hereditary thrombocytopenia]. Ugeskr Laeger 1987;149:2332–3.

36. Joensuu H, Kankaanranta L, Seppala T, Auterinen I, Kallio M, Kulvik M, et al. Boron neutron capture therapy of brain tumors: clinical trials at the finnish facility using boronophenylalanine. J Neurooncol 2003;62: 123–34.
37. Kageji T, Mizobuchi Y, Nagahiro S, Nakagawa Y, Kumada H. Clinical results of boron neutron capture therapy (BNCT) for glioblastoma. Appl Radiat Isot 2011; 69:1823–5.
38. Miyatake SI, Kawabata S, Hiramatsu R, Kuroiwa T, Suzuki M, Ono K. Boron Neutron Capture Therapy of Malignant Gliomas. Prog Neurol Surg 2018;32: 48–56.
39. Sander A, Wosniok W, Gabel D. Case numbers for a randomized clinical trial of boron neutron capture therapy for Glioblastoma multiforme. Appl Radiat Isot 2014;88:16–9.
40. Thyss R, Virolle V, Imbert V, Peyron JF, Aberdam D, Virolle T. NF-kappaB/Egr-1/Gadd45 are sequentially activated upon UVB irradiation to mediate epidermal cell death. EMBO J 2005;24:128–37.
41. Boone DN, Qi Y, Li Z, Hann SR. Egr1 mediates p53-independent c-Myc-induced apoptosis via a noncanonical ARF-dependent transcriptional mechanism. Proc Natl Acad Sci U S A 2011;108:632–7.
42. Ye JM, Deng T, Zhang JB. Influence of paeonol on expression of COX-2 and p27 in HT-29 cells. World J Gastroenterol 2009;15:4410–4.
43. Akao Y, Nakagawa Y, Iinuma M, Nozawa Y. Anti-cancer effects of xanthones from pericarps of mangosteen. Int J Mol Sci 2008;9:355–70.
44. Watanapokasin R, Jarinthanan F, Nakamura Y, Sawasjirakij N, Jaratrungtawee A, Suksamrarn S. Effects of α-Mangostin on apoptosis induction of human colon cancer. World J Gastroenterol 2011;17:2086–95.